Vietnam Journal of Earth Sciences, 45(2), 147-163, https://doi.org/10.15625/2615-9783/18206

Vietnam Journal of Earth Sciences
https://vjs.ac.vn/index.php/jse

Analysis of gravity data for extracting structural features of the northern region of the Central Indian Ridge

Luan Thanh Pham[1, *], K.N.D. Prasad[2]

[1]*University of Science, Vietnam National University, Hanoi, Vietnam*
[2]*CSIR-National Geophysical Research Institute, Hyderabad, India*

Received 21 October 2022; Received in revised form 14 December 2022; Accepted 22 March 2023

ABSTRACT

In this study, structural lineaments and fracture zones of the northern region of the Central Indian Ridge have been determined using gravity data from XGM2019e_2159 global gravity model. In this scope, firstly, the edge detection performances of the gradient amplitude of the tilt angle (THDR), theta map (TM), improved local phase (ILP), and improved logistic (IL) methods have been evaluated on synthetic examples. The results show that the IL method effectively avoids false edges and produces high-resolution edges. Then, the methods are applied to the gravity anomaly of the northern region of the Central Indian Ridge. It has been determined that the most prominent structural lineaments observed over the region are in the NE-SW and NW-SE directions. These trends match reasonably with the significant trends of the Tilt depth solutions that show a depth range of 2.2 km to 7 km for different geological structures. In addition, the obtained results are compatible with the known fracture zones of the study area. The findings help us to improve our understanding of the structure and tectonic framework of the study region.

Keywords: gravity, edge detection, structural feature, Central Indian Ridge.

1. Introduction

The Central Indian Ridge is a prominent structure of the Western Indian Ocean (Fig. 1a). The study on the formation, evolution and growth of oceanic crust along the Central Indian Ridge will help to better comprehend the tectonic and geodynamic evolution of the Western Indian Ocean (Sahoo et al., 2022a, b). The structural boundaries are related to discontinuities or contacts among the different formations (Dwivedi and Chamoli, 2021). In the past, some investigations were conducted to improvise the knowledge of the evolution process of the Central Indian Ridge (i.e., McKenzie and Scalter, 1971; Fisher et al., 1971; Patriat and Segoufin, 1988; Cochran et al., 2003; Dick et al., 2003). However, most of the results obtained from these investigations were based on bathymetric and magnetic data. Although some seismic and potential field studies were performed elsewhere in the Indian Ocean, the northern part of the Central Indian Ridge is poorly explored. It is well known that

*Corresponding author, Email: luanpt@hus.edu.vn

gravity data are used in various applications, including the study of various geodynamic/tectonic processes and oil and gas exploration (Oksum, 2021; Ghomsi et al., 2022a, b). Recently, some studies based on interpreting gravity data were carried out to describe structural lineaments of the Central Indian Ridge. For example, Sahoo and Pal (2019) applied the tilt angle methods to gravity data from the EIGEN 6C4 model to map crustal lineament pattern in the Central Indian Ridge, Sahoo et al. (2022a, b) applied the normalized standard deviation and normalized gradient amplitude to gravity anomaly from the marine gravity model to determine the lineaments in the area. Since their studies cover extensive regions, the determined structure images in the north Central Indian Ridge have a low-resolution.

Many methods have been introduced to outline the structures from the gravity anomaly (Eldosouky et al., 2022a). These edge enhancement methods evolve with the use of the derivatives of gravity data (Ekinci et al., 2013; Kafadar, 2017; Ghomsi et al., 2022c). Cordell (1979) first used the gradient amplitude maxima to recognize the source edges. This method has been applied in many studies to extract geological formations (Ekinci and Yiğitbaş, 2015; Pilkington and Tschirhart, 2017). An improved modification of the horizontal gradient has been used by Fedi and Florio (2001). They developed a technique that employs higher-order gradients to minimize the interference effects caused by nearby sources. Roest et al. (1992) showed that the analytical signal peaks can determine the source' horizontal boundaries. Many researchers have used the analytic signal to enhance subsurface structural features (Saibi et al., 2016, 2019; Hang et al., 2017). Hsu et al. (1996) improved the resolution of the analytic signal using the second-order gradients of the data. Gravity data contains signals having a wide anomaly amplitude range, and the low amplitudes may be considered valuable geological elements. However, it is difficult to recognize the low amplitudes among the higher amplitudes when using the horizontal gradient, analytic signal, and their enhanced versions (Eldosouky et al., 2022b).

Over the past few decades, many methods have been introduced to enhance deep and shallow structures (Pham et al., 2022a). For the first time, Miller and Singh (1994) pioneered the development of the balanced edge detector called the “tilt angle,” which brought a balanced image for different source depths but could not delineate the source boundaries. Verduzco et al. (2004) showed that the tilt angle gradient clearly highlights the boundaries. Wijns et al. (2005) introduced the theta map, which normalizes the total horizontal gradient by the analytic signal. Cooper and Cowan (2008) proposed using the normalized standard deviations to balance the anomaly amplitudes due to shallow and deep sources. Cooper (2009) suggested using the balanced edge detector based on the analytical signal and its Hilbert transforms. Ma and Li (2012) used the normalized gradient amplitude to improve deep source results. Ma (2013) proposed using the improved local phase technique that combines derivatives with different orders to display the boundaries more precisely. Cooper (2014) introduced the tilt angle of the analytic signal to balance the strong and weak anomaly amplitudes. Zhang et al. (2015) showed that using the tilt angle of the high-order gradients shows the edges more clearly. Yuan et al. (2016) proposed using the modified theta that fully uses the measured gradient components. Nasuti Y and Nasuti A.

(2018) introduced an improved version of the tilt angle to improve its edge detection ability. To increase the result resolution, Pham et al. (2018, 2019a) developed some methods using the logistic functions of the analytical signal. Since the logistic methods are less effective in mapping the boundaries of the thin bodies, their modified versions have been introduced by replacing the analytic signal with the gradient amplitude (Pham et al., 2019b, 2020). Oksum et al. (2021) proposed using a fast sigmoid function technique to balance the strong and weak anomaly amplitudes. Kafadar (2022) suggested using the Kuwahara filter to bring more clearly edges and detailed results compared to the traditional methods. Recently, Prasad et al. (2022a, 2022b) introduced balanced methods using the derivatives of the gradient amplitude to enhance the edge detection resulting from the deep-seated sources.

In this study, we applied the horizontal gradient of the tilt angle (THDR), theta map (TM), improved local phase (ILP) and improved logistic (IL) methods to high-resolution gravity data from the XGM2019e_2159 global gravity model to the study region in the north Central Indian Ridge to recognize density boundaries in the area. The obtained results help us to have a clear understanding of the Nature, structure, and tectonic framework of the study region.

2. Geology and Tectonics

The location of the studied region in the north Central Indian Ridge and its bathymetry map are shown in Figs. 1a and 1b, respectively. The fracture zones in the study region, reported by Wessel et al. (2015), are marked in Fig. 1b by solid black lines. The plate tectonic evolution of the Central Indian Ocean started in the Late Cretaceous (A29) (Patriat and Segoufin, 1988). The Central Indian Ocean is developed due to the rifting and subsequent drifting of the Gondwanaland fragments. The relative motions between these fragments resulted in the evolution of critical structural features, namely the Crozet basin, the Madagascar basin, and the western and eastern parts of the Central Indian basin (Yatheesh et al., 2019). The western Indian Ocean marks the presence of the Rodrigues Triple Junction (RTJ), where the African, Indo-Australian, and Antarctic plates meet and is considered a stable triple junction (McKenzie and Sclater, 1971; Fisher et al., 1971). The RTJ came into existence during the Late Cretaceous period (64 Ma) when the Seychelles plate drifted away from the Indian plate, which led to the formation of the Carlsberg Ridge (Fig. 1a). The Central Indian Ridge (the boundary between the African and Indo-Australian plates), Southwest Indian Ridge (the boundary between the African and the Antarctic plates), and Southeast Indian Ridge (the boundary between the Antarctic and the Indo-Australian plates) form an integral part of the RTJ in the Indian Ocean (Tapscott et al., 1980). The central Indian basin is located on the eastern side of the Central Indian Ridge. In contrast, the western portion is covered by the Reunion, Mauritius, the Mascarene Islands, and the Mascarene basin (Fig. 1a). Reunion, Mauritius, and the Mascarene Islands are wholly volcanic edifices (Fisher et al., 1967). The Mascarene Islands form a volcanic archipelago in the Southern Indian Ocean stretching from Reunion Island for about 1000 km, situated on the aseismic part of the central Indian Ocean. Mauritius Island, lying on the southern extension of the Mascarene Plateau, is an eroded complex volcanic pile surrounded by a narrow shelf and barrier reefs dated in the

Tertiary age. Mauritius Island shows the same regional trend (bathymetry) as the Mascarene Plateau, with a large central volcano rising 5000 m above the sea floor (McDougall and Chamalaun, 1969). The Reunion Island is a volcanic pile separated by a distance of 170 km west-southwest of Mauritius Island. The Reunion Island represents the second largest volcanic island of the Mascarene archipelago with 2.1 Ma old data lavas (Hantke and Scheidegger, 1998). Since the Southeast Indian Ridge extends from the RTJ (25.5°S, 70.0°E) to the Macquarie Ridge Complex in the southeast of Australia, it has the fastest spreading rates among the three arms of the RTJ, controls the present opening of the Indian Ocean (Royer and Schlich, 1988). The Southwest Indian Ridge spreads slowly at 14 mm/year and is related to cold mantle temperatures and thick lithosphere representing an end-member in the global mid-oceanic ridge system (DeMets et al., 1990). The Central Indian Ridge is a slow-intermediate spreading-rate plate boundary at 43 mm/year (DeMets et al., 1994; Royer et al., 1997; Muller et al., 1993).

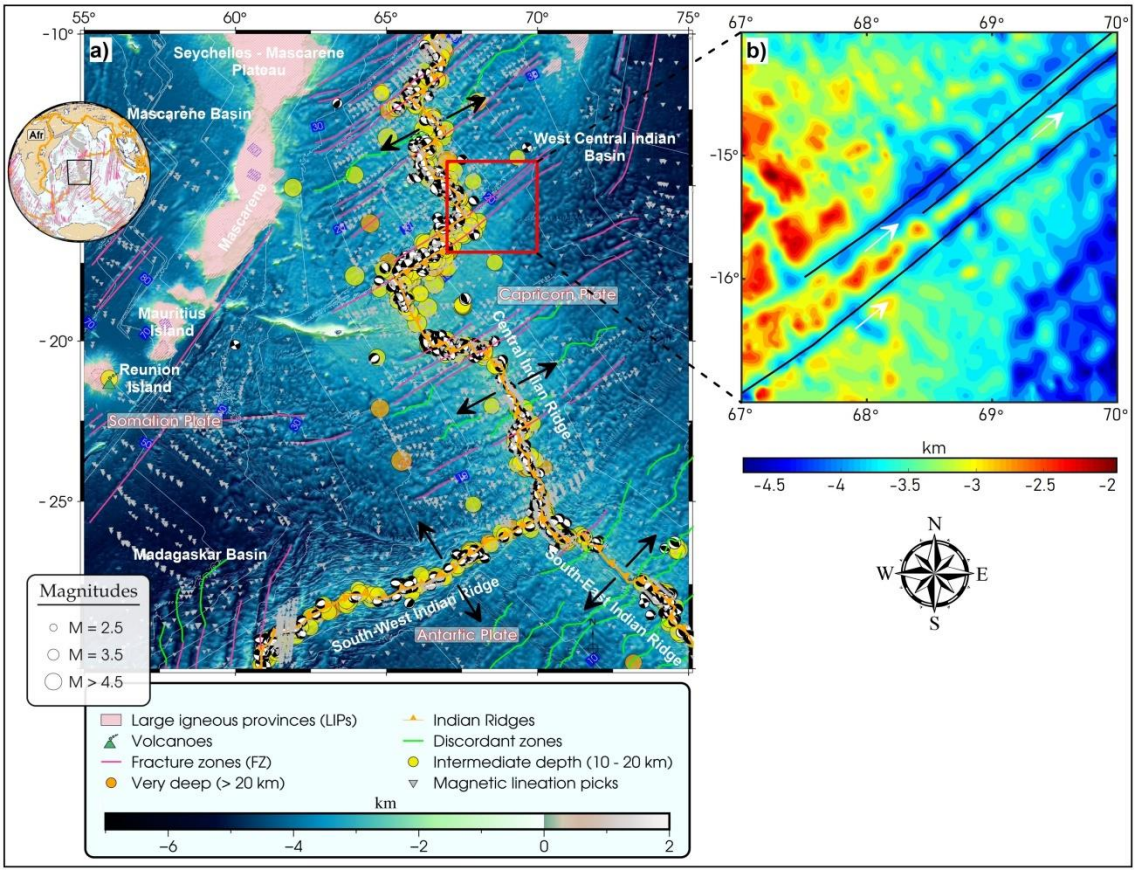

Figure 1. a) Geodynamic framework of the Central Indian Ocean, b) Bathymetry the study area. The study area is marked by a red box. The fracture zones reported by Wessel et al. (2015) are displayed by red and black lines in Fig. 1a and 1b, respectively

3. Methods

Verduzco et al. (2004) presented the THDR filter using peak locations to map the boundaries. It is defined as:

$$THDR = \sqrt{\left(\frac{\partial TA}{\partial x}\right)^2 + \left(\frac{\partial TA}{\partial y}\right)^2}. \quad (1)$$

where the tilt angle (TA) of the field (F) is given by:

$$TA = tan^{-1}\left(\frac{\frac{\partial F}{\partial z}}{\sqrt{\left(\frac{\partial F}{\partial x}\right)^2 + \left(\frac{\partial F}{\partial y}\right)^2}}\right). \quad (2)$$

The TM filter normalizes the gradient amplitude and provides the minimum values over the edges. The TM can be stated as follows (Wijns et al., 2005):

$$\mathrm{TM} = cos^{-1}\left(\frac{\sqrt{\left(\frac{\partial F}{\partial x}\right)^2 + \left(\frac{\partial F}{\partial y}\right)^2}}{\sqrt{\left(\frac{\partial F}{\partial x}\right)^2 + \left(\frac{\partial F}{\partial y}\right)^2 + \left(\frac{\partial F}{\partial z}\right)^2}}\right). \quad (3)$$

The ILP is formed by calculating the different order derivatives of gravity data. The method is known as an improved local phase method. The maximum values detect the edges of the density structures in the ILP map. The ILP is given by (Ma, 2013):

$$\mathrm{ILP} = sin^{-1}\left(\frac{\sqrt{\left(\frac{\partial F}{\partial x}\right)^2 + \left(\frac{\partial F}{\partial y}\right)^2}}{\sqrt{\left(\frac{\partial F}{\partial x}\right)^2 + \left(\frac{\partial F}{\partial y}\right)^2 + \left(\left(\frac{\partial^2 F}{\partial x^2} + \frac{\partial^2 F}{\partial y^2}\right)\frac{mean\left(\frac{\partial F}{\partial z}\right)}{mean\left(\frac{\partial^2 F}{\partial z^2}\right)}\right)^2}}\right). \quad (4)$$

The IL is another method that uses the peak locations to outline the edges of the density structures. It uses the horizontal gradient and improves on the method of Pham et al. (2018). The IL equation is given by (Pham et al., 2020):

$$\mathrm{IL} = \frac{1}{1 + \exp[-\mathrm{p}(\mathrm{R_{HG}} - 1) + 1]}, \quad (5)$$

where $2 \le \mathrm{p} \le 5$ (Pham et al., 2020) and $\mathrm{R_{HG}}$ is given by:

$$\mathrm{R_{HG}} = \frac{\frac{\partial \mathrm{HG}}{\partial \mathrm{z}}}{\sqrt{\left(\frac{\partial \mathrm{HG}}{\partial \mathrm{x}}\right)^2 + \left(\frac{\partial \mathrm{HG}}{\partial \mathrm{y}}\right)^2}}, \quad (6)$$

where the horizontal gradient (HG) is given by (Cordell, 1979):

$$\mathrm{HG} = \sqrt{\left(\frac{\partial \mathrm{F}}{\partial \mathrm{x}}\right)^2 + \left(\frac{\partial \mathrm{F}}{\partial \mathrm{y}}\right)^2}. \quad (7)$$

4. Synthetic model study

Before applying the THDR, TM, ILP, and IL techniques to the accurate data, we must test their feasibility. A synthetic model is designed to evaluate the effectiveness of the methods (Fig. 2a). Table 1 shows the parameters of the bodies of the synthetic model. The model gravity anomaly is computed and displayed in Fig. 2b.

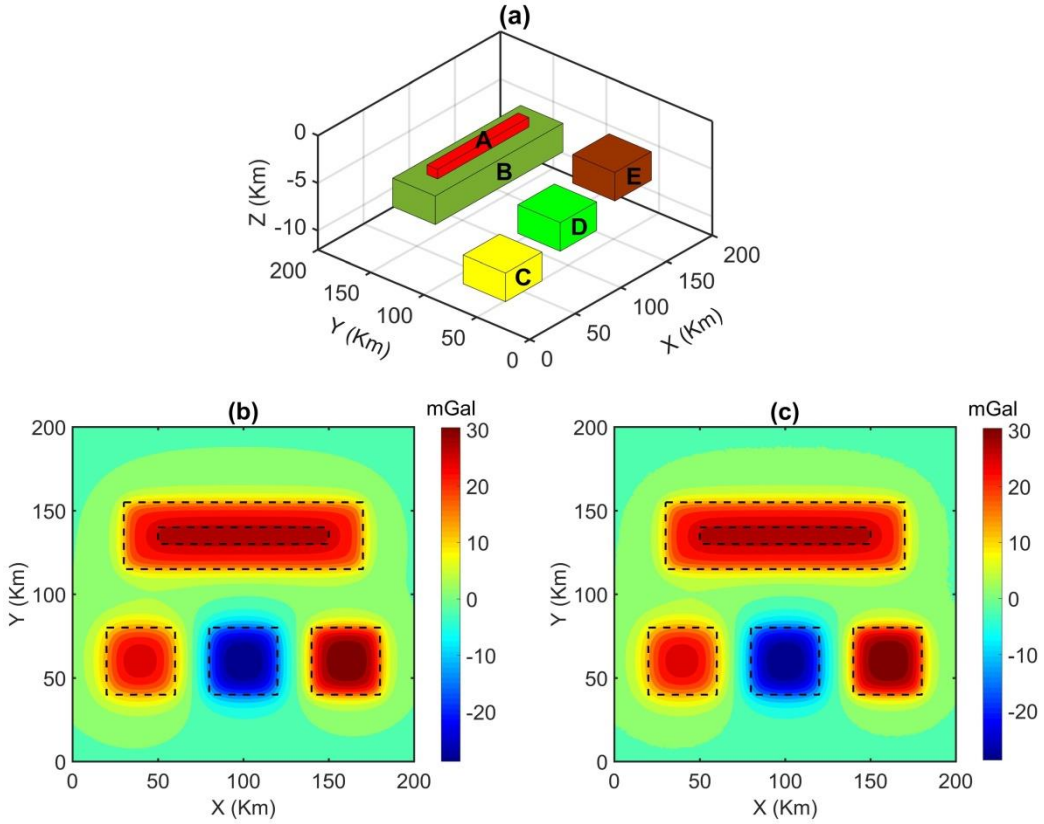

Figure 2. a) Synthetic model, b) synthetic gravity data,
b) synthetic gravity data with noise. Dashed lines show the true edges

Table 1. Parameters of the bodies

Parameters	A	B	C	D	E
Coordinates of center (km, km)	100; 135	100; 135	40; 60	100; 60	160; 60
Width (km)	10	40	40	40	40
Length (km)	100	140	40	40	40
Top depth (km)	3	4	8	6	4
Bottom depth (km)	4	7	11	9	7
Density contrast (g/cm^3)	0.17	0.25	0.35	-0.35	0.35

Figure 3a displays the edges determined using the THDR method. As shown in this figure, the THDR is predominate by the responses of high amplitude signals from the shallow structures B and E, but the low amplitude responses from the deep-seated bodies C and D are blurred. Besides, the THDR produces spurious maxima around the body D. Fig. 3b displays the edges determined using the TM method. As observed, this technique is more effective than the THDR in bringing balanced edges, but it cannot detect the edges of body A. Similar to the THDR, the TM also generates spurious boundaries around body D. Moreover, the locations of the minimum values obtained from the TM for the deepest body C are shifted out from the natural edges. Fig. 3c presents the edges estimated by the ILP technique. Although the ILP has

much sharper gradients over the edges than the THDR and TM, it also produces artifacts around the bodies A and D. In addition, the ILP does not provide a clear image for the edges of the body A. Fig. 3d depicts the edges estimated by the IL. This figure shows that the IL provides excellent estimates of all the edges with different depths. This method can bring the edges in a high resolution without any spurious edges.

To test the noise sensitivity of the THDR, TM, ILP, and IL methods, we added 3% Gaussian noise to the gravity data. Fig. 2c presents noise-corrupted gravity data. Figs. 4a-4d represent the results of the THDR, TM, ILP, and IL techniques, respectively. We can observe that the response from the THDR filter is more sensitive to noise when compared with the TM, ILP and IL filtering techniques.

Moreover, the edges obtained from this technique are very faint. In this case, the IL still estimates all the source edges. This method brings clearer and more accurate edges compared to other methods.

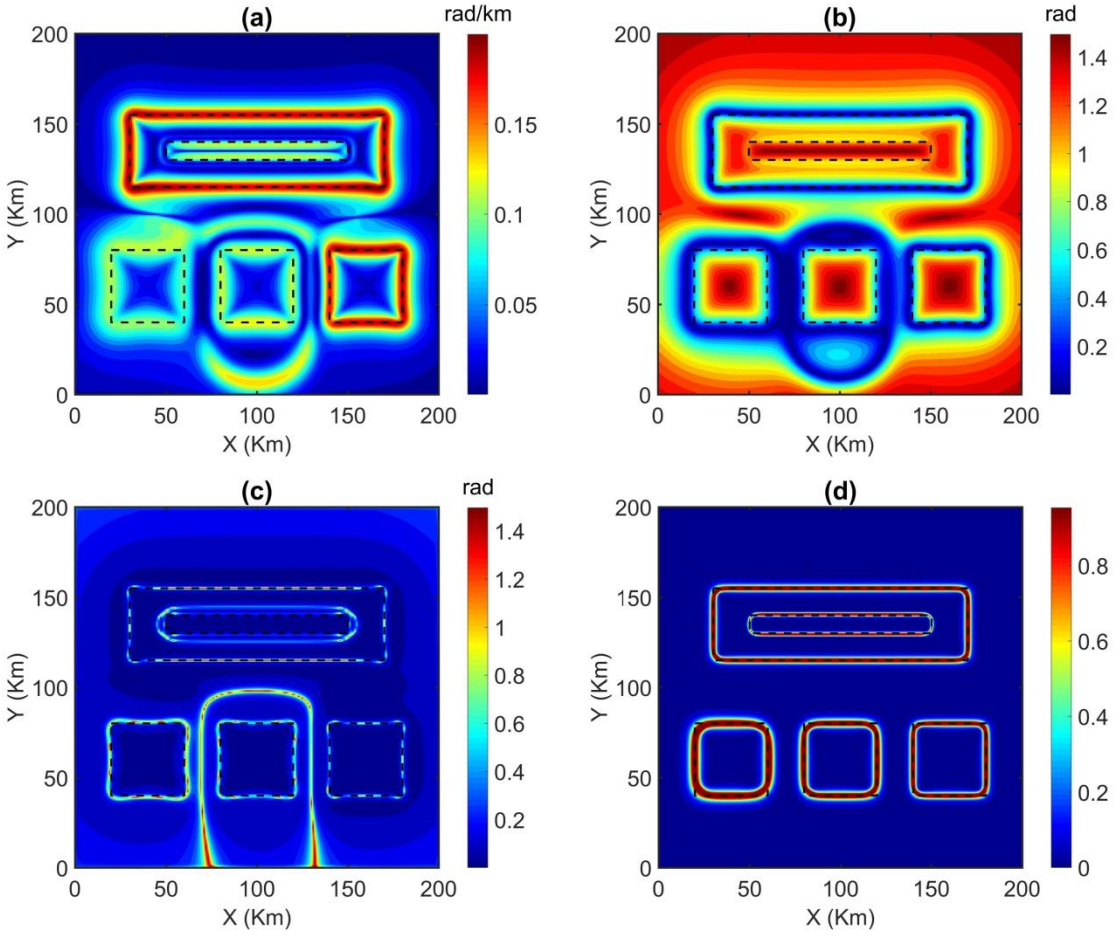

Figure 3. a) THDR, b) TM, c) ILP, d) IL of the gravity anomaly. Dashed lines show the true edges

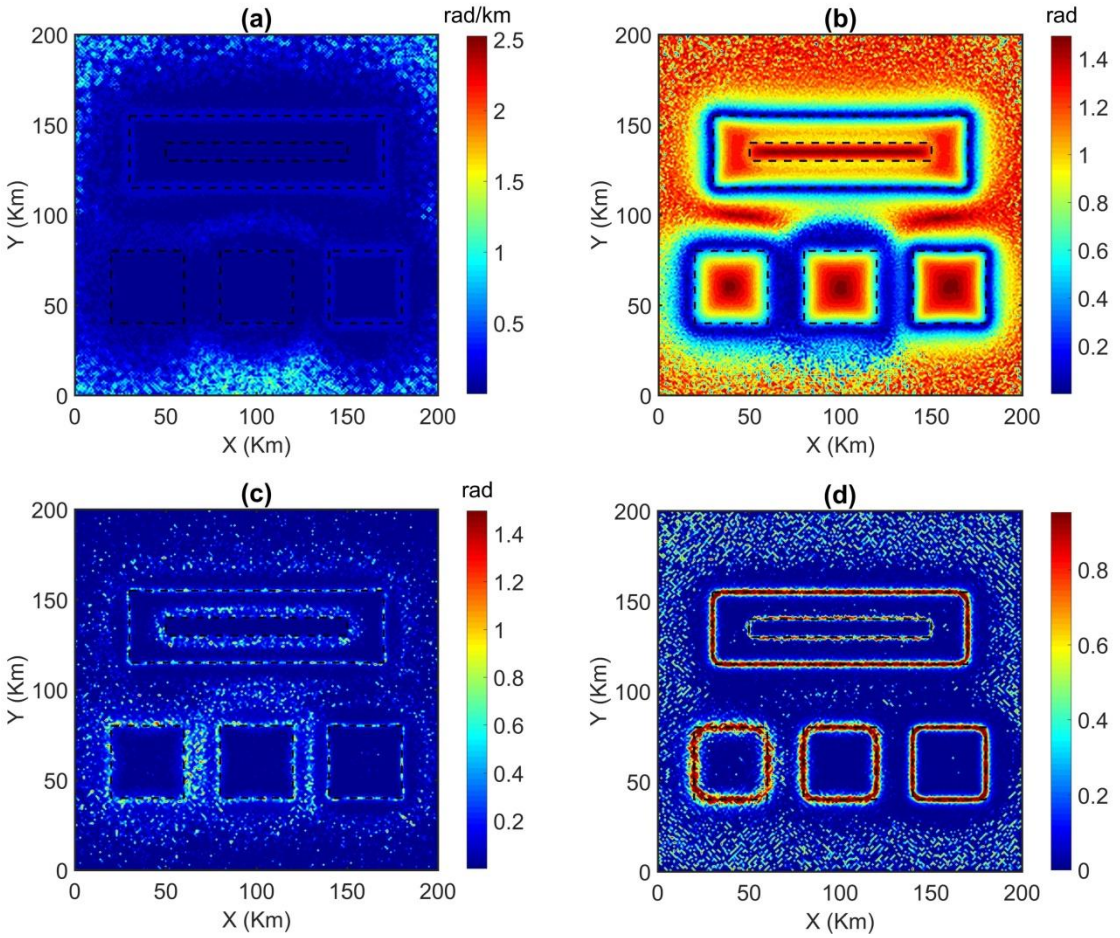

Figure 4. a) THDR, b) TM, c) ILP, d) IL of the noisy gravity anomaly. Dashed lines show the true edges

5. Data

The Global Gravity Models (GGMs) provide helpful information to the various geoscience disciplines such as geophysics, oceanography, glaciology, hydrology, and climatology, which play a critical role in understanding and gaining knowledge related to the shape of the Earth and its internal structure, mass transport and distribution, glacial isostasy, continental hydrology, and sea level changes. There are many recently developed GGMs, such as EGM2008 (Pavlis et al., 2012), EIGEN6C4 (Förste et al., 2014), GECO (Gilardoni et al., 2016), XGM2016 (Pail et al., 2018), and XGM2019e_2159. These models are classified based on the model and type of acquisition. The former is sub-classified as satellite-only (e.g., CHAMP, GRACE, GRACE-Follow-On, GOCE, GRAIL, etc.) and satellite plus the data acquired by terrestrial, airborne, ship, and altimetry gravity observations. And the latter is sub-classified as static and time-variable gravity data. However, the data's better spatial and temporal resolution accuracy is achieved by combining the satellite data from altimetry satellites and data from terrestrial, marine, and airborne gravity measurements.

The XGM2019e_2159 is a GGM with spherical harmonics at degree and order 5399, corresponding to a resolution of about 4 km (Zingerle et al., 2019). The XGM2019e_2159

experimental gravity model includes GOCO06s for the longer wavelength measurements combined with terrestrial measurements (data over land (EARTH2014) and ocean (DTU13) of gravity anomalies provided by courtesy of NGA augmented with topographically derived gravity over land) for the shorter wavelengths up to degree and order 719 (15'). The XGM2019e can perform better than the other GGMs in the regions where the terrestrial data gap exists. Studies like Apeh and Tenzer (2022) and Yuan et al. (2022) established that XGM2019e_2159 performs better than EIGEN-6C4 and par with EGM2008 GGM. Apeh and Tenzer (2022) mimicked major geological boundaries better than other GGMs in the Afikpo Basin, South Africa. Nzeuga et al. (2022) also used gravity data from this model to determine the geological structures in Southwestern Cameroon. The satellite-based global gravity models are well-suited for delineating structural maps in regions where in-situ data determination is difficult (Pal et al., 2016a, b; Pham et al., 2019c; 2021, 2022b, c; Melouah et al., 2021). The present work uses the XGM2019e_2159 model with a resolution of about 4 km (Zingerle et al., 2020) to delineate the pseudo-tectonic map over the study region near Central Indian Ridge (latitude between 14°-17°S and longitude between 67°-70°E). High-resolution bathymetry data (Fig. 1) and XGM2019e_2159 Free-air and Bouguer data of the studied region are generated from the International GEBCO and Centre for Global Earth Models, respectively. The free-air and Bouguer gravity anomalies of the studied region in the Central Indian Ridge are shown in Figs. 5a and 5b, respectively. In this area, the free-air anomaly broadly ranges between -50 to 60 mGal, whereas the Bouguer gravity anomalies range between 174-319 mGal. The high-amplitude Bouguer gravity anomalies are observed towards the north-eastern region of the study area, and the low-amplitude Bouguer anomalies are found in the western region of the area (Fig. 5b).

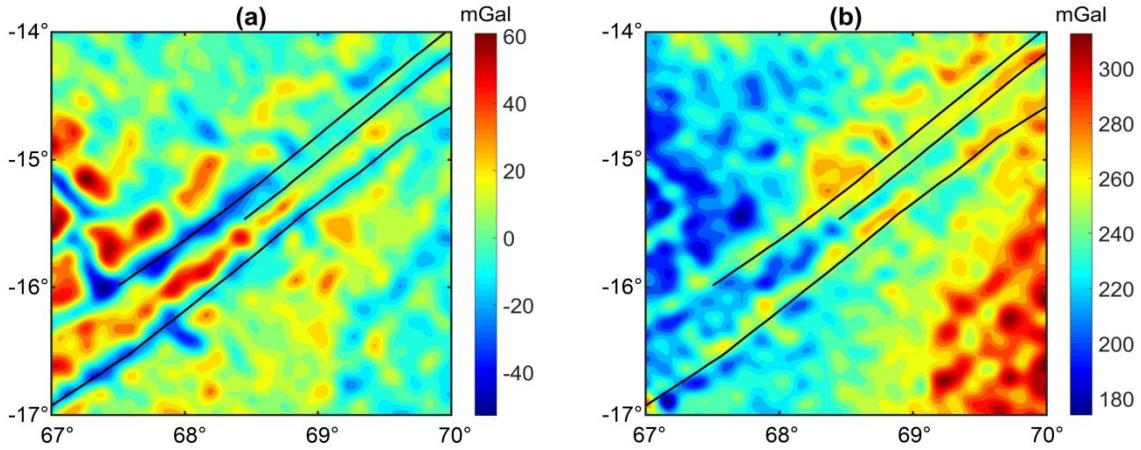

Figure 5. a) Free-air gravity anomaly, b) Bouguer gravity anomaly of the study region. Black lines show the fracture zones

6. Results

The Bouguer gravity data from XGM2019e (degree 2159) model is used to extract a new structural map of the studied area. The lineaments delineated using the THDR, TM, ILP and IL are shown in Figs. 6a, 6b, 6c and 6d, respectively and are overlaid by the existing tectonic features (solid black lines on

the subsets of Fig. 6). Even though most of the lineament features were detected by the THDR, the signal is not balanced effectively (Fig. 6a). The delineated lineaments by the TM are closely connected each other that makes the interpretation difficult (Fig. 6b) and a similar issue is found with the ILP (Fig. 6c). The lineament map generated with the use of IL is shown in Fig. 6d that proves to be a better filter when compared to the above discussed techniques. The study region mostly comprises lineaments trending in random directions and spread all over the study region (Fig. 6d). The north-west corner consists of lineaments trending mostly in NW-SE followed by NNW-SSE. The north-east corner of the map is found with NE-SW trending lineaments followed by almost E-W trending lineaments on either side of the former lineaments. Similarly, the southeast corner of the studied region is found with NE-SW trending lineaments that are mostly linear, and some are partly curvilinear. The southwest corner of the map is observed mostly with NE-SW trending lineaments followed by patches of NW-SE trending lineaments. The region along the NE-SW zone at the center of the map shows the minimum possible correlation with the existing tectonic features. The existing tectonics are marked by continuous linear tectonic features whereas the delineated new structural features are marked with discontinuous linear trends with a spectacular correlation along the spreading zones.

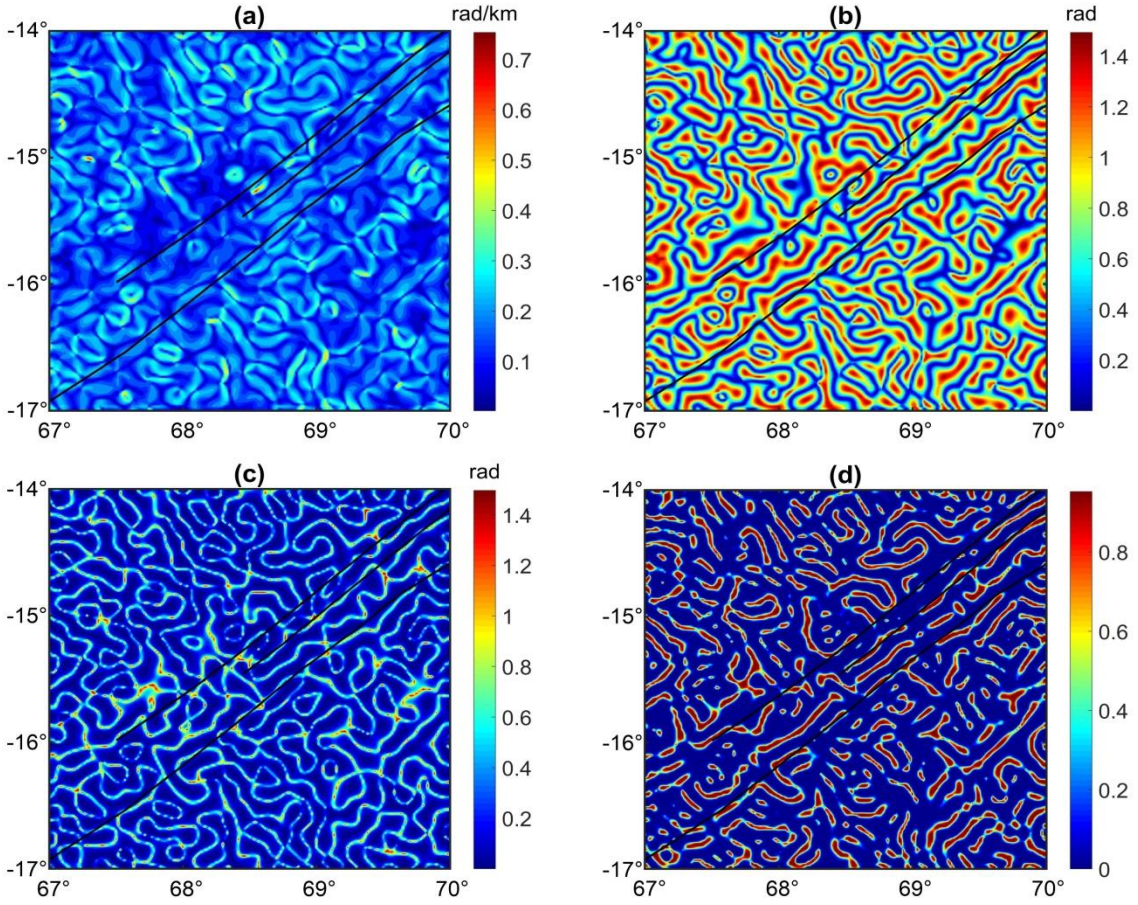

Figure 6. a) THDR, b) TM, (c) ILP, d) IL of Bouguer gravity data. Black lines show the fracture zones

Once the structural trends in the studied region are extracted using the IL method, we further proceed to estimate the top depth of these structural features using the second-order Tilt_depth method (Oruc, 2011). The depth map of various structural features observed in the studied region is shown in Fig. 7a. The depth of these structural features varies between 2-7 km, being distributed randomly all over the study region. The histogram of the computed lineament depth map is shown in Fig. 7b, which depicts that 70% of these lineaments exist at 3-5 km depth.

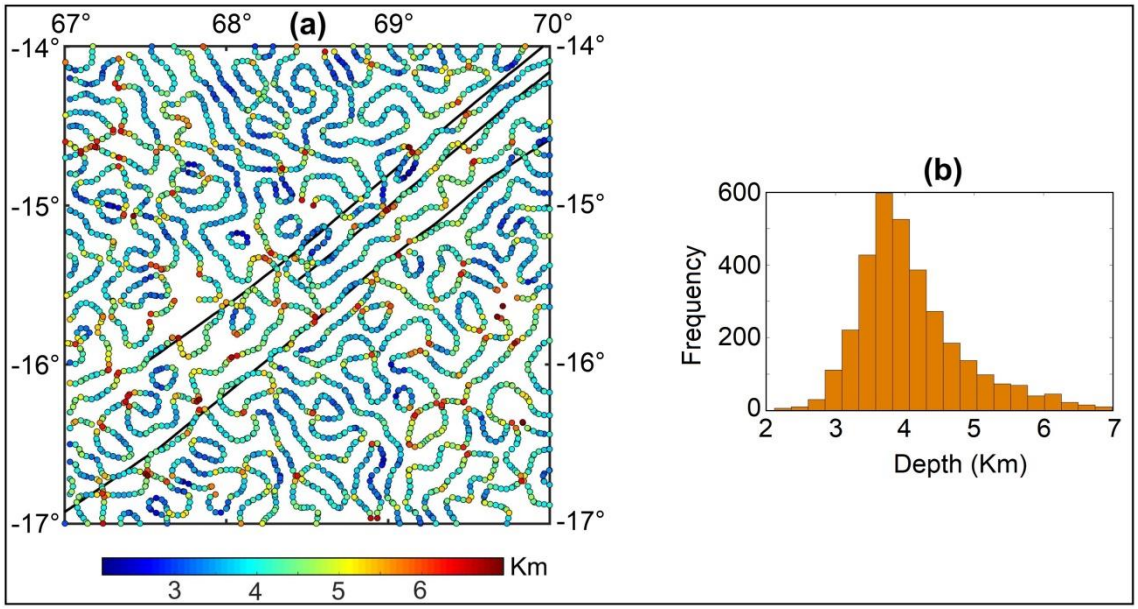

Figure 7. a) The depths from the second order Tilt_depth method,
b) Histogram of the depth estimates. Black lines show the fracture zones

7. Discussions

The IL method is used to demarcate the boundaries of the geological features and these features are overlaid on the base map of the studied region (Fig. 8). Although the THDR does not bring a balanced image of the edges, and the edges obtained from the TM and ILP methods are connected, the presence of most of gravity lineaments in the IL map is also verified by the signals of the THDR, TM and ILP (Fig. 6). By comparing the results in Figs. 7a and 8, we can see that the structural trends from the IL method match reasonably with the major trends of the Tilt_depth solutions. However, unlike the solutions of the Tilt_depth method, the IL can delineate the structural lineaments and fracture zones more clearly without any connected structures. This finding illustrates the helpfulness of the IL technique for gravity data interpretation. As discussed in section 4, the IL method cannot only delineate the true edges, but it can also be able to avoid any spurious and fallacious edges that are produced by noise in the data. As shown in Fig. 8, three fracture zones in the region are clearly illustrated by the IL method. The IL method is also useful in highlighting a wide range of structural features of the northern region of the Central Indian Ridge. However, it is noteworthy that the fracture zones reported by Wessel et al. (2015) in the area were derived from bathymetry data interpretation, while the use of the gravity anomaly can extract both surface and subsurface structures. Therefore, the additional boundaries may respond to

deeper sources, which do not show signs on the ocean bottom. It is well known that the slower tectonic activity generates more lineaments leading a high lineament density (Casas et al., 2000). Our results show a high lineament density in the study region (Fig. 8), indicating that the Central Indian Ridge is a slow spreading ridge.

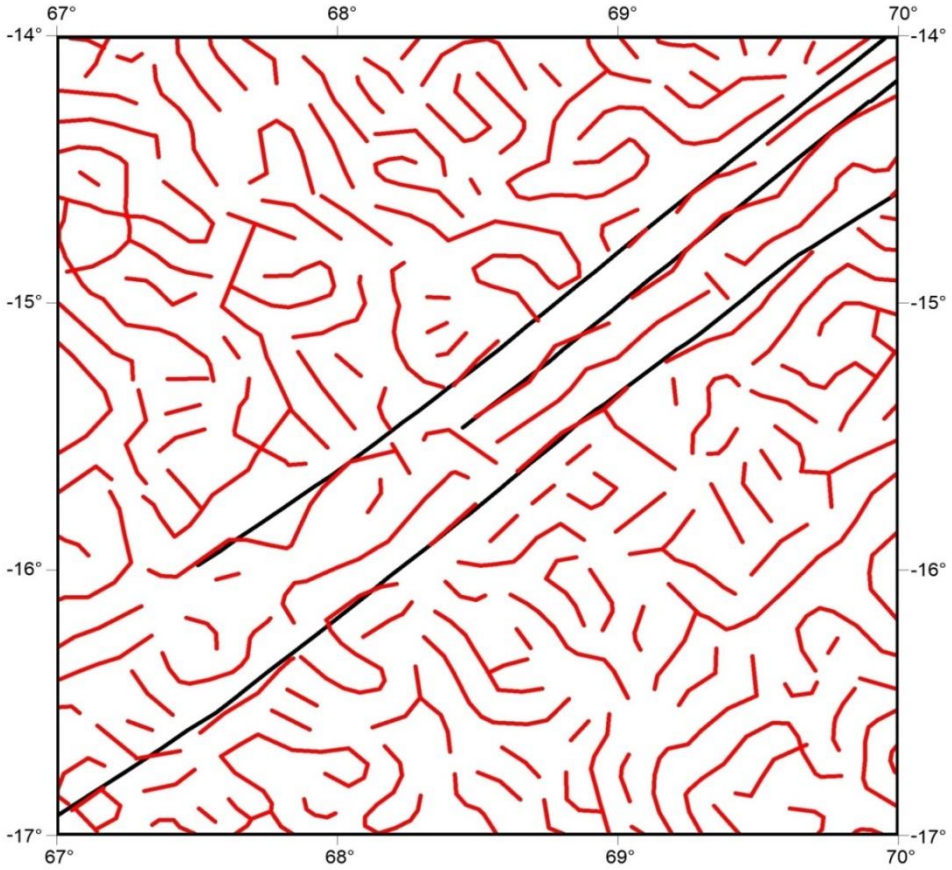

Figure 8. Structural map derived from the IL method. Black lines show the fracture zones

In general, earthquakes along the Central Indian Ridge axis are related to strike-slip and normal faults (Fig. 1a). Indeed, Radha Krishna and Verma (2000) carried out a detailed interpretation of earthquakes along the Central Indian Ridge through a comparison of the seismicity pattern with different morphotectonic segments of the ridge. Their study showed that focal mechanisms for strong earthquakes occurring along the ridge largely show either strike-slip motion on steeply dipping nodal planes parallel to the transform, or normal faulting with one of the nodal planes parallel to the local spreading segment. As shown in Fig. 1a, most of the normal faulting occurs near the RTJ. The uniform distribution of the strike-slip faulting along the ridge axis indicates that most of the tectonic movements occurring near the Central Indian Ridge are in the NW-SE and NE-SW and directions. We can see that most of the structural lineaments observed in the north Central Indian Ridge are also predominantly oriented in the NW-SE and NE-SW directions (Fig. 8). The formation of the NE-SW trending lineaments, representing the current spreading direction, could probably be due to the shift in plate

movement to a more NE direction along the Central Indian Ridge (Sahoo et al., 2022b). The presence of long NE-SW lineaments is possibly associated with the slow spreading rate along the Central Indian Ridge during the Early and Late Eocene (Patriat and Segoufin, 1988), while short lineaments in the NE-SW direction point towards a relatively high spreading rate during the Early Eocene as reported by Sahoo et al. (2022b). On the other hand, the lineaments in the NW-SE direction were the result of the ridge jump occurred during the anomaly 20 and 18 (Patriat and Segoufin, 1988; Sahoo and Pal, 2019). Mellor (1998) showed that this jump resulted in forming of many sub-parallel linear volcanic ridges and lines on the crust closer to the Central Indian Ridge. The upwelled mantle material, of volcanic origin, at these structures is denser and so, the gravity anomalies at these structures are found to have relatively high amplitude. Some of the NW-SE trending lineaments are related to the orientation of the present-day Central Indian Ridge axis. In addition, a few of these lineaments are also related to breaking continuity in the long lineaments oriented in the NE-SW direction (Fig. 8). Note that the NW-SE trending lineaments were not mapped by the analysis of magnetic data reported by Patriat and Segoufn (1988).

One of the recent studies by Sahoo et al. (2022a) gave a lineament map generated by the normalized standard deviation method, which is dependent on the window size. Due to the selected window being large, most of the small lineaments in various directions along the spreading axis of the Central Indian ridge were not detected which finds a major concern in the lineament density and fractal estimates of Sahoo et al. (2022a). The low fractal dimension and lineament density values computed by Sahoo et al. (2022a) over the present study region (Middle block) indicate a greater uniformity in the lineament distribution, which could need a new interpretation based on the present study results. Here, the present study is successful in enhancing the quality of the structural map and producing a clear image of the sub-surface features. Most of the structural lineaments observed in the IL map (Fig. 8) are related to the extensional ridge tectonic process observed all along the Central Indian Ridge. Since much of the study region is disturbed by an extreme lithospheric deformation and the diffuse tectonic Nature of the plate boundaries separating the three main plates, i.e., Somalian, Antarctic and Capricorn (Patriat, 1987; Yatheesh et al., 2019) (Fig. 1a), there is a possibility of multiple and random folding and faulting that is clearly visible in the generated tectonic map. As discussed in earliest studies (e.g., Weissel et al., 1980; Zuber, 1987), the present study confirms the presence of the crustal folding with basement features that are parallel Moho structures and block faulting along the Central Indian Ridge.

8. Conclusions

We have applied the THDR, TM, ILP and IL methods to high-resolution gravity data from the XGM2019e_2159 model to determine the structural lineaments and fracture zones of the northern region of the Central Indian Ridge. Model studies were performed to consider the major problems of the boundary determination methods before applying these techniques to the Bouguer anomaly of the studied region. The findings show that the IL method is more effective than other methods in bringing high-resolution edges and avoiding false information. The results also showed that the structural lineaments in the NE-SW and NW-SE directions are dominant in the area. The NE-SW trending lineaments represent the current spreading direction of the Central Indian Ridge, whereas NW-SE trending lineaments were the result of the ridge jump occurred during the anomaly 20 and 18. These lineaments present a good correlation with the

Tilt_depth solutions. Moreover, the obtained density boundaries are also in accord with the known fracture zones in the northern region of the Central Indian Ridge. The derived structural map provided the extension of the major structural features along the ridge axis. These findings could probably aid in better understanding the geology and tectonics of the Central Indian Ridge.

Acknowledgements

We sincerely thank Franck Eitel Kemgang Ghomsi from National Institute of Cartography, Cameroon for proving Fig. 1a used in this study. We greatly appreciate constructive comments of the editor Phan Trong Trinh and three anonymous reviewers. Luan Thanh Pham was funded by Vingroup JSC and supported by the Postdoctoral Scholarship Programme of Vingroup Innovation Foundation (VINIF), Vingroup Big Data Institute (VinBigdata), code VINIF.2022.STS.43

References

Apeh O.I., Tenzer R., 2022. Selection of an optimum global gravitational model for geological mapping of Afikpo and Anambra Basins in Nigeria. Geodesy and Cartography, 48(2), 92-106.

Bruinsma S.L., Förste C., Abrikosov O., Lemoine J.M., Marty J.C., Mulet S., Rio M.H., Bonvalot S., 2014. ESA's satellite-only gravity field model via the direct approach based on all GOCE data. Geophysical Research Letters, 41(21), 7508-7514.

Casas A.M., Cortes A.L., Maestro A., Soriano M.A., Riaguas A., Bernal J., 2000. LINDENS: A program for lineament length and density analysis. Computers and Geosciences, 26(9-10), 1011-1022.

Cochran J.R., Kurras G.J., Edwards M.H., Coakley B.J., 2003. The Gakkel Ridge: Bathymetry, gravity anomalies, and crustal accretion at extremely slow spreading rates. Journal of Geophysical Research-Solid Earth, 108, 1978-2012.

Cooper G.R.J., 2009. Balancing images of potential-field data. Geophysics, 74(3), L17-L20.

Cooper G.R.J., 2014. Reducing the dependence of the analytic signal amplitude of aeromagnetic data on the source vector direction. Geophysics, 79, J55-J60.

Cooper G.R.J., Cowan D.R., 2008. Edge enhancement of potential-field data using normalized statistics. Geophysics, 73, H1-H4.

Cordell L., 1979. Gravimetric expression of graben faulting in Santa Fe country and the Espanola Basin. In: 30th Field conference New Mexico, New Mexico Geological Society Guidebook, 59-64.

DeMets C., Gordon R.G., Argus D.F., Stein S., 1990. Current plate motions. Geophysical Journal International, 101(2), 425-478.

Demets C., Gordon R.G., Vogt P., 1994. Location of the Africa-Australia-India triple junction and motion between the Australian and Indian plates: Results from an aeromagnetic investigation of the Central Indian and Carlsberg ridges. Geophysical Journal International, 119(3), 893-930.

Dick H.J.B., Lin J., Schouten H., 2003. An ultras low spreading class of ocean ridge, Nature, 426, 405-412.

Dwivedi D., Chamoli A., 2021. Source edge detection of potential field data using Wavelet decomposition. Pure and Applied Geophysics, 178(3), 919-938.

Ekinci Y.L., Ertekin C., Yiğitbaş E., 2013. On the effectiveness of directional derivative based filters on gravity anomalies for source edge approximation: synthetic simulations and a case study from the Aegean graben system (western Anatolia, Turkey). Journal of Geophysics and Engineering, 10(3), 035005.

Ekinci Y.L., Yiğitbaş E., 2015. Interpretation of gravity anomalies to delineate some structural features of Biga and Gelibolu peninsulas, and their surroundings (north-west Turkey). Geodinamica Acta, 27(4), 300-319.

Eldosouky A.M., Pham L.T., Duong V.H., Ghomsi F.E.K., Henaish A., 2022a. Structural interpretation of potential field data using the enhancement techniques: a case study. Geocarto International. Doi: 10.1080/10106049.2022.2120548.

Eldosouky A.M., Pham L.T., Henaish A., 2022b. High precision structural mapping using edge filters of potential field and remote sensing data: A case study from Wadi Umm Ghalqa area, South Eastern Desert, Egypt. The Egyptian Journal of Remote Sensing and Space Science, 25(2), 501-513.

Fedi M., Florio G., 2001. Detection of potential fields source boundaries by enhanced horizontal derivative method. Geophysical Prospecting, 49(1), 40-58.

Fisher R.L., Johnson G.L., Heezen B.C., 1967. Mascarene Plateau, Western Indian Ocean.

Geological Society of America Bulletin, 78(10), 1247-1266.

Fisher R.L., Sclater J.G., McKenzie D.P., 1971. Evolution of the central Indian ridge, western Indian Ocean. Geological Society of America Bulletin, 82(3), 553-562.

Förste C., Bruinsma S., Abrikosov O., Lemoine J., Schaller T., Götze H., Balmino G., 2014. EIGEN-6C4. The latest combined global gravity field model including GOCE data up to degree and order, 2190, 5th GOCE User Workshop, Paris, 1-29.

Gilardoni M., Reguzzoni M., Sampietro D., 2016. GECO: a global gravity model by locally combining GOCE data and EGM2008. Stud. Geophy. et Geod., 60, 228-247.

Ghomsi F.E.K., Pham L.T., Steffen R., Ribeiro-Filho N., Tenzer R., 2022c. Delineating structural features of North Cameroon using EIGEN6C4 high-resolution global gravitational model. Geological Journal, 1-15.

Ghomsi F.E.K., Pham L.T., Tenzer R., Esteban F.D., Vu T.V., Kamguia J., 2022b. Mapping of fracture zones and structural lineaments of the Gulf of Guinea passive margins using marine gravity data from CryoSat-2 and Jason-1 satellites. Geocarto International. Doi: 10.1080/10106049.2022.2040602.

Ghomsi F.E.K., Tenzer R., Njinju E., Steffen R., 2022a. The crustal configuration of the West and Central African Rift system from gravity and seismic data analysis. Geophysical Journal International, 230(2), 995-1012.

Hang N.T., Thanh D.D., Minh L.H., 2017. Application of directional derivative method to determine boundary of magnetic sources by total magnetic anomalies. Vietnam Journal of Earth Science, 39(4), 360-375.

Hantke R., Scheidegger A.E., 1998. Morphotectonics of the Mascarene Islands. Annali Di Geofisica, 41(2), 165-180.

Hsu S.K., Sibuet J.C., Shyu C.T., 1996. High-resolution detection of geologic boundaries from potential field anomalies: an enhanced analytic signal technique. Geophysics, 61(2), 373-386.

Kafadar Ö., 2017. CURVGRAV-GUI: a graphical user interface to interpret gravity data using curvature technique. Earth Sci Inform., 10(4), 525-537.

Kafadar Ö., 2022. Applications of the Kuwahara and Gaussian filters on potential field data, Journal of Applied Geophysics, 104583.

Kostelecky J., Klokocník J., Bucha B., Bezdek A., Förste C., 2015. Evaluation of gravity field model EIGEN-6C4 by means of various functions of gravity potential, and by GNSS/levelling. Geoinformatics Fce Ctu, 14(1), 7-28.

Ma G., 2013. Edge detection of potential field data using improved local phase filter. Explor. Geophys., 44(1), 36-41

Ma G., Li L., 2012. Edge detection in potential fields with the normalized total horizontal derivative. Comput. Geosci., 41, 83-87.

McDougall I.A.N., Chamalaun F.H., 1969. Isotopic dating and geomagnetic polarity studies on volcanic rocks from Mauritius, Indian Ocean. Geological Society of America Bulletin, 80(8), 1419-1442.

McKenzie D.P., Sclater J.G., 1971. The evolution of the Indian Ocean since the Late Cretaceous. Geophys. Jour. Roy. Astr. Soc., 25, 437- 528.

Mellor S.H., 1998. The geochemistry and petrology of the Rodrigues Ridge (Western Indian Ocean), PhD Thesis, University of Greenwich.

Melouah O., Eldosouky A.M., Ebong W.D., 2021. Crustal architecture, heat transfer modes and geothermal energy potentials of the Algerian Triassic provinces, Geothermics, 96, 102211.

Miller H.G., Singh V., 1994. Potential field tilt a new concept for location of potential field sources. Journal of Applied Geophysics, 32, 213-217.

Muller R.D., Royer Y.J., Lawver L.A., 1993. Revised plate motions relative to the hotspots from combined Atlantic and Indian Ocean hotspot tracks, Geology, 21, 275-278.

Nasuti Y., Nasuti A., 2018. NTilt as an improved enhanced tilt derivative filter for edge detection of potential field anomalies. Geophysical Journal International, 214(1), 36-45.

Nzeuga A.R., Ghomsi F.E., Pham L.T., Eldosouky A.M., Aretouyap Z., Kana J.D., Yasmine Z.T., Fokem A.B.K., Nouayou R., Abdelrahman K., Fnais M.S., Andráš P., 2022. Contribution of advanced edge detection methods of potential field data in the tectono-structural study of the southwestern part of Cameroon. Frontiers in Earth Science, 10, 970614.

Oksum E., 2021. Grav3CH_inv: a GUI-based MATLAB code for estimating the 3-D basement depth structure of sedimentary basins with vertical and horizontal density variation. Computers and Geoscience, 155, 104856.

Oksum E., Le D.V., Vu M.D., Nguyen T.H.T., Pham L.T., 2021. A novel approach based on the fast sigmoid function for interpretation of potential field

data. Bulletin of Geophysics and Oceanography, 62(3), 543-556.

Oruc B., 2011. Edge Detection and Depth Estimation Using a Tilt Angle Map from Gravity Gradient Data of the Kozaklı-Central Anatolia Region, Turkey. Pure and Applied Geophysics, 168, 1769-1780.

Pail R., Bruinsma S., Migliaccio F., Förste C., Goiginger H., Schuh W.D., Höck E., Reguzzoni M., Brockmann J.M., Abrikosov O., Veicherts M., 2011. First GOCE gravity field models derived by three different approaches. Journal of Geodesy, 85(11), 819-843.

Pail R., Fecher T., Barnes D., Factor J.F., Holmes S.A., Gruber T., Zingerle P., 2018. Short note: the experimental geopotential model XGM2016. Journal of geodesy, 92(4), 443-451.

Pal S.K., Majumdar T.J., Pathak V.K., Narayan S., Kumar U., Goswami O.P., 2016a. Utilization of high-resolution EGM2008 gravity data for geological exploration over the Singhbhum-Orissa Craton, India. Geocarto International, 31(7), 783-802.

Pal S.K., Narayan S., Majumdar T.J., Kumar U., 2016b. Structural mapping over the 85°E Ridge and surroundings using EIGEN6C4 highresolution global combined gravity field model: an integrated approach. Marine Geophysical Research, 37(3), 159-184.

Patriat P., 1987. Reconstruction of the evolution of the Indian Ocean ridge system using plate cidmatics methods. Aust Lands. Antarctica. Fr. (Mission Rech.), Paris, 308.

Patriat P., Segoufin J., 1988. Reconstruction of the central Indian ocean, Tectonophysics, 155(1-4), 211-234.

Pavlis N.K., Holmes S.A., Kenyon S.C., Factor J.K., 2012. The development and evaluation of the Earth Gravitational Model 2008 (EGM2008). Journal of Geophysical Research: Solid Earth, 117(B04406), 1-38.

Pham L.T., Do T.D., Oksum E., Le S.T., 2019c. Estimation of Curie point depths in the Southern Vietnam continental shelf using magnetic data. Vietnam Journal of Earth Science, 41(3), 216-228.

Pham L.T., Kafadar O., Oksum E., Hoang-Minh T., 2022a. A comparative study on the peak detection methods used to interpret potential field data: A case study from Vietnam. Geocarto International, 37(13), 3679-3696.

Pham L.T., Oksum E., Do T.D., 2019b. Edge enhancement of potential field data using the logistic function and the total horizontal gradient. Acta Geodaetica et Geophysica, 54, 143-155.

Pham L.T., Oksum E., Do T.D., Le-Huy M., 2018 New method for edges detection of magnetic sources using logistic function. Geofizichesky Zhurnal, 40(6), 127-135.

Pham L.T., Oksum E., Do T.D., Le-Huy M., Vu M.D., Nguyen V.D., 2019a. LAS: a combination of the analytic signal amplitude and the generalised logistic function as a novel edge enhancement of magnetic data. Contributions to Geophysics and Geodesy, 49(4), 425-440.

Pham L.T., Oksum E., Eldosouky A.M., Gomez-Ortiz D., Abdelrahman K., Altinoğlu F.F., Nguyen T.N., 2022c. Determining the Moho interface using a modified algorithm based on the combination of the spatial and frequency domain techniques: a case study from the Arabian Shield. Geocarto International. Doi: 10.1080/10106049.2022.2037733.

Pham L.T., Oksum E., Kafadar O., Trinh P.T., Nguyen D.V., Vo Q.T., Le S.T., Do T.D., 2022b. Determination of subsurface lineaments in the Hoang Sa islands using enhanced methods of gravity total horizontal gradient. Vietnam Journal of Earth Sciences, 44(3), 395-409.

Pham L.T., Ghomsi F.F.K., Vu T.V., Oksum E., Steffen R., Tenzer R., 2022c. Mapping the structural configuration of the western Gulf of Guinea using advanced gravity interpretation methods. Physics and Chemistry of the Earth, 129 (2023) 103341.

Pham L.T., Oliveira S.P., Le M.H., Trinh P.T., Vu T.V., Duong V.H., Ngo T.N.T., Do T.D., Nguyen T.H., Eldosouky A.M., 2021e. Delineation of structural lineaments of the Southwest Sub-basin (East Vietnam Sea) using global marine gravity model from CryoSat-2 and Jason-1 satellites. Geocarto International, 1-18. Doi: 10.1080/10106049.2021.1981463.

Pham L.T., Vu T.V., Le Thi S., Trinh P.T., 2020. Enhancement of potential field source boundaries using an improved logistic filter. Pure and Applied Geophysics, 177(11), 5237-5249.

Pilkington M., Tschirhart V., 2017. Practical considerations in the use of edge detectors for geologic mapping using magnetic data. Geophysics, 82(3), J1-J8.

Prasad K.N.D., Pham L.T., Singh A.P., 2022a. Structural mapping of potential field sources

using BHG filter. Geocarto International, 1-28. Doi: 10.1080/10106049.2022.2048903.

Prasad K.N.D., Pham L.T., Singh A.P., 2022b. A novel filter "ImpTAHG" for edge detection and a case study from Cambay Rift Basin, India. Pure and Applied Geophysics, 179(6-7), 2351-2364.

Radha Krishna M., Verma R.K., 2000. Seismotectonics of the Central Indian Ridge, western Indian Ocean. Journal of the Geological Society of India, 55(5), 515-527.

Roest W.R., Verhoef J., Pilkington M., 1992. Magnetic interpretation using the 3-D analytic signal. Geophysics 57, 116-125.

Royer J.Y., Schlich R., 1988. Southeast Indian Ridge between the Rodriguez Triple junction and Saint-Paul islands: Detailed kinematics for the past 20 m.y. Journal of Geophysical Research, 93, 13524-13550.

Royer J.Y., Gordon R.G., DeMets C., Vogt P.T., 1997. New limits on the motion between India and Australia since Chron 5 (11 Ma) and implications for lithospheric deformation in the equatorial Indian Ocean. Geophysical Journal International, 129, 41-53.

Royer J.Y., Schlich R., 1988. Southeast Indian Ridge between the Rodriguez triple junction and the Amsterdam and Saint-Paul islands: Detailed kinematics for the past 20 my. Journal of Geophysical Research: Solid Earth, 93(B11), 13524-13550.

Sahoo S., Narayan S., Pal S.K., 2022a. Fractal analysis of lineaments using CryoSat-2 and Jason-1 satellite-derived gravity data: Evidence of a uniform tectonic activity over the middle part of the Central Indian Ridge, Physics and Chemistry of the Earth, 128, 103237.

Sahoo S., Narayan S., Pal S.K., 2022b. Appraisal of gravity-based lineaments around Central Indian Ridge (CIR) in different geological periods: Evidence of frequent ridge jumps in the southern block of CIR. Journal of Asian Earth Sciences, 239, 105393.

Sahoo S.D., Pal S.K., 2019. Mapping of Structural Lineaments and Fracture Zones around the Central Indian Ridge (10°S-21°S) using EIGEN 6C4 Bouguer Gravity Data. J. Geol. Soc. India, 94(4), 359-366.

Saibi H., Amir G., Mohamed F.S., 2019. Subsurface structural mapping using gravity data of AlAin region, Abu Dhabi Emirate, United Arab Emirates. Geophysical Journal International, 216(2), 1201-1213.

Saibi H., Azizi M., Mogren S., 2016. Structural investigations of Afghanistan deduced from remote sensing and potential field data. Acta Geophysica, 64(4), 978-1003.

Tapscott C.R., Patriat P., Fisher R.L., Sclater J.G., Hoskins H., Parsons B., 1980. The Indian Ocean triple junction. Journal of Geophysical Research: Solid Earth, 85(B9), 4723-4739.

Verduzco B., Fairhead J.D., Green C.M., MacKenzie C., 2004. New insights into magnetic derivatives for structural mapping. The Leading Edge, 23, 116-119.

Weissel J.K., Anderson R.N., Geller C.A., 1980. Deformation of the Indo-Australian plate. Nature, 287(5780), 284-291.

Wessel P., Matthews K.J, Müller R.D., Mazzoni A., Whittaker J.M., Myhill R., Chandler M.T, 2015. Semi-automatic fracture zone tracking. Geochemistry Geophysics Geosystems, 16, 2462-2472.

Wijns C., Perez C., Kowalczyk P., 2005. Theta map: Edge detection in magnetic data. Geophysics, 70, 39-43.

Yatheesh V., Dyment J., Bhattacharya G.C., Royer J.Y., Kamesh Raju K.A., Ramprasad T., Chaubey A.K., Patriat P., Srinivas K., Choi Y., 2019. Detailed structure and plate reconstructions of the Central Indian Ocean between 83.0 and 42.5 Ma (Chrons 34 and 20). Journal of Geophysical Research: Solid Earth, 124(5), 4305-4322.

Yuan H., Wan X., Wu Y., Peng Y., Guo Z., 2022. Evaluation of ultra-high degree gravity field models: a case study of Eastern Tibetan Plateau and Sichuan Province. Terrestrial, Atmospheric and Oceanic Sciences, 33(1), 1-12.

Yuan Y., Gao J.Y., Chen L.N., 2016. Advantages of horizontal directional Theta method to detect the edges of full tensor gravity gradient data. Journal of Applied Geophysics, 130, 53-61.

Zhang X., Yu P., Tang R., Xiang Y., Zhao C.J., 2015. Edge enhancement of potential field data using an enhanced tilt angle. Exploration Geophysics, 46(3), 276-283.

Zingerle P., Pail R., Gruber T, Oikonomidou X., 2020. The combined global gravity field model XGM2019e. Journal of Geodesy, 94(7), 1-12.

Zuber M.T., 1987. Compression of oceanic lithosphere: An analysis of intraplate deformation in the Central Indian Basin. Journal of Geophysical Research: Solid Earth, 92(B6), 4817-4825.